Eur. Phys. J. D **44**, 133–139 (2007)
DOI: 10.1140/epjd/e2007-00168-7

THE EUROPEAN PHYSICAL JOURNAL D

Formation and stabilisation of single current filaments in planar dielectric barrier discharge

L. Stollenwerk[1,a], Sh. Amiranashvili[1,b], J.-P. Boeuf[2], and H.-G. Purwins[1]

[1] Institut für Angewandte Physik, Corrensstraße 2/4, 48149 Münster, Germany
[2] CPAT, Université Paul Sabatier, 118 route de Narbonne, 31062 Toulouse Cedex 4, France

Received 15 December 2006 / Received in final form 13 April 2007
Published online 23 May 2007 – © EDP Sciences, Società Italiana di Fisica, Springer-Verlag 2007

Abstract. In the experimental part we report on a typical bifurcation scenario of the current distribution in the discharge plane of a planar dielectric barrier discharge system. Increasing the amplitude $\hat{U}$ of the sinusoidal driving voltage after breakdown a large number of dynamic solitary filaments is observed and the subsequent decrease of $\hat{U}$ results in a pronounced hysteresis with decreasing number of filaments. In this way isolated single stationary filaments can be generated. In the theoretical part the latter are modeled by a reaction-drift-diffusion equation that is solved in three dimensional space numerically without any fitting procedure. As a result we obtain well defined stationary filaments of which size an shape essentially are independent of the initial conditions and having a width and an amplitude that agree with experiment rather well. On the basis of the numerical results we consider mechanisms of filament stabilisation. This includes the discussion of the well known surface charges as well as an additional focusing effect of volume charges.

PACS. 52.65.-y Plasma simulation – 52.80.Hc Glow; corona – 89.75.Kd Patterns – 89.75.Fb Structures and organization in complex systems

1 Introduction

Dielectric barrier discharge (DBD) systems play an important role in many technical applications, like plasma display panels, ozone generation and environmental techniques [8]. Due to the rich amount of patterns in the discharge, DBD are also of great scientific interest within the field of Nonlinear Dynamics and Pattern Formation [1,3,5,7,11,18], where the usual set-up consists of two plane-parallel electrodes. Among other things, commonly observed patterns consist of an arrangement of single, a few, or many current filaments. The filaments within one pattern usually have all the same size and shape and are independent of the boundary conditions. The patterns are stable for many thousand driver periods, i.e. the dynamic of the pattern takes places on a much slower timescale [18]. Filamentary patterns occur over a very wide range of parameters. Therefore the generation of current filaments is a generic phenomenon and of considerable interest. Thereby the understanding of the single current filament is the necessary basis for the understanding of all the complex filamentary patterns that are observed.

However, so far there are only few theoretical works about self-organised patterns in DBD systems. A qualitative description of a stabilising mechanism based on the surfaces charges on the dielectric barriers is given in [4]. To our knowledge the only quantitative descriptions of the filamentation process are given in [9,11], which are calculated in 2D, and in [16], which describes the filamentation process in full 3D space. In this work we want to introduce a numerical investigation on the long-time stability of a single filament in a planar DBD system. The often used radial (r, z) coordinates are not sufficient in this case, as they hide non-radial instabilities, that are important in this work. Instead, we perform a full 3D simulation.

In the experimental part (Sect. 2) we want to describe a typical experimental set-up and some basic properties of the discharge (Sect. 2.1). In Section 2.2 we present a typical experimental bifurcation scenario and how to prepare a single filament in the experiment. In the theoretical part (Sect. 3) of this article we first introduce the model and then (in Sect. 3.1) we demonstrate numerically that our model is able to reproduce the experimentally observed filament correctly. Finally, in Section 3.2, we analyse the mechanisms of stabilisation of a single filament.

2 Experimental system

The set-up of a typical experiment is shown in Figure 1. The system consists of two parallel glass plates with the thickness $a = 0.5$–1 mm. On the outer side they are

[a] e-mail: stollenw@uni-muenster.de
[b] *Present address*: Weierstraß-Institut für Angewandte Analysis und Stochastik, Mohrenstraße 39, 10117 Berlin, Germany.

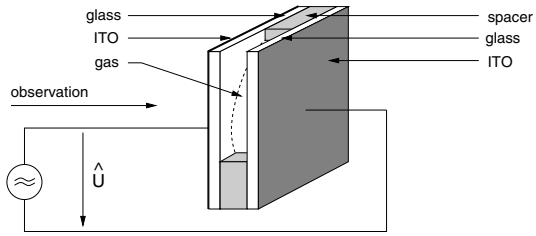

Fig. 1. Typical experimental set-up. Two glass plates of thickness a are separated by a spacer defining a circular gas-discharge space being filled with a gas at pressure p and having the discharge length d and the diameter D. On the outside the glass plates are coated with ITO which represents the metallic electrodes. Through one of them the gas discharge can be observed via the emitted luminescence radiation density using sufficiently fast cameras. The system is driven by a sinusoidal high voltage supply with frequency f and amplitude $\hat{U}$.

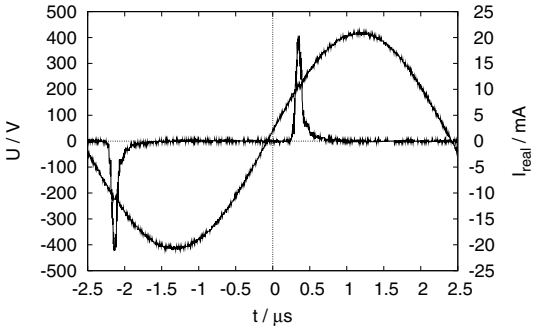

Fig. 2. Typical evolution of voltage and real-current. There is one real-current peak per half-period of the driving voltage. *Parameters:* $a = 0.5$ mm, $d = 0.5$ mm, $D = 40$ mm, $p = 200$ hPa, $f = 200$ kHz, helium.

covered with a transparent and electroconductive ITO (indium tin oxide) layer. The spacer between the glass plates has the thickness $d = 0.5$–1 mm and defines a circular discharge area with the diameter $D = 5$–50 mm. The working gas may be helium, argon or nitrogen at a pressure $p = 100$–500 hPa. The ITO electrodes are connected to an a.c. power supply providing a sinusoidal voltage with the frequency $f = 50$–500 kHz and the amplitude $\hat{U}$ up to approximately 1000 V. The discharge may be observed through the transparent ITO layer. Great care has been taken to provide for homogeneous conditions in the discharge plane.

2.1 Characterisation of the discharge

Figure 2 shows the typical evolution of voltage and real-current in the discharge system. The reactive current due to the capacitive load of the discharge system is separated off using a Wheatstone-bridge. Both for a homogeneous and a filamentary discharge there is only a single real-current peak per half-period of the driving voltage. The discharge is a classical ac glow-discharge (definition e.g. [14]).

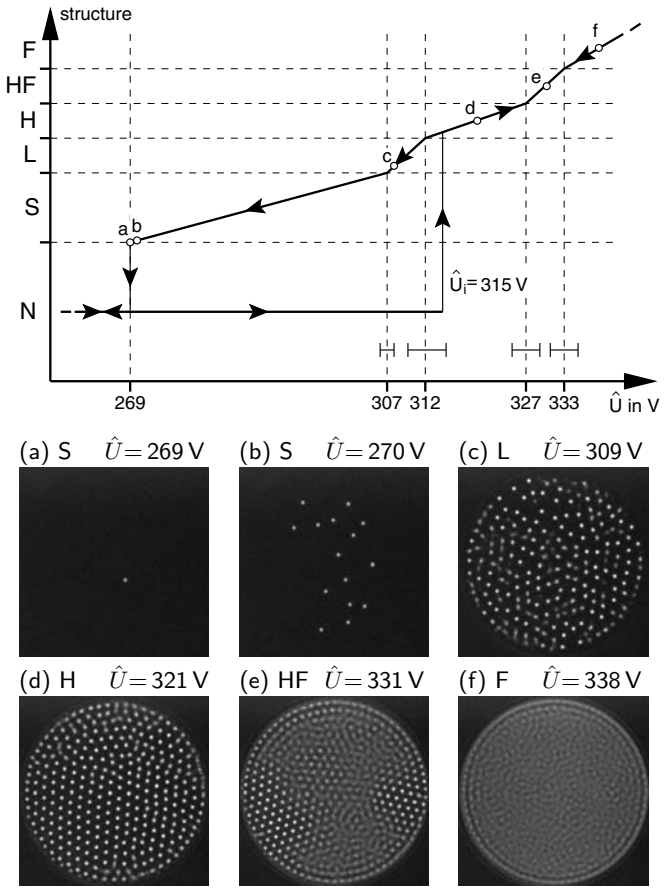

Fig. 3. Typical experimentally observed bifurcation scenario. The upper part shows the bifurcation diagram with the observed structure against the driving voltage $\hat{U}$. The structures are N: no pattern, S: single filaments, L: loose arrangement, H: hexagonal arrangement, HF: areas with hexagonal arranged and fast moving filaments, F: fast moving filaments. $\hat{U}_i$ is the ignition voltage of the system. The letters a–f depict the according images (a)–(f) below. *Parameters:* $a = 0.5$ mm, $d = 0.5$ mm, $D = 40$ mm, $p = 200$ hPa, $f = 200$ kHz, helium, $t_{\mathrm{exp}} = 1/250$ s.

2.2 Bifurcation behaviour

A typical bifurcation scenario obtained in systems like those depicted in Figure 1 is shown in Figure 3. Thereby the amplitude $\hat{U}$ is increased starting at $\hat{U} = 0$ V. As soon as the ignition voltage for the first breakdown $\hat{U}_i = 315$ V is reached, the gas discharge ignites. The first few breakdowns are nearly homogeneous, but after about 10 breakdowns a many filament pattern is generated, that, depending on the surface properties of the dielectrics, may move erratically. A detailed examination of the process of filamentation can be found in [16]. As the emerging gas-discharge acts as an additional load for the voltage supply, the driving voltage amplitude decreases to approximately 310 V after ignition. Therefore, instead of the hexagonal pattern H a loose arrangement L of filaments is observed. The filaments are all of the same size of approximately 1 mm full width at half height. The filament size varies

only little with the discharge parameters. For a higher driving voltage or a higher gas pressure the filaments become slightly smaller.

As the driving voltage is increased additional filaments are generated and filaments organise in a hexagonal arrangement (H) at ≈311 V. In this experiment the hexagonal pattern is static[1], but there are experimental conditions leading to the motion of the whole pattern or parts of it [17]. Passing ≈328 V areas containing fast moving filaments arise (HF). With an exposure time t_{exp} of 1/250 s they appear blurred in the images (Fig. 3e). With increasing driving voltage the areas containing fast dynamics grow, and at ≈333 V all filaments are in fast motion and the pattern appears blurred (F). In all the discussed patterns the system operates in the glow mode and the time dependence of the applied voltage and the current response is typically of the form Figure 2.

In Figure 3 we also depict the scenario that follows by decreasing $\hat{U}$. During the decrease first the same patterns as before appear in reverse order until we reach $\hat{U} \approx 307$ V. In this region the bifurcations occur within the measuring uncertainty at the same voltages as for increasing driving voltage. If the driving voltage is decreased below ≈307 V also the short-range order gets lost, so we refer to these structures as single filaments (S). The single filaments are stable over a wide range of the driving voltage. In this situation according to surface conditions the filaments may move or stay at rest. However, the lower the driving voltage is, the higher is the probability that some filaments extinguish spontaneously. If the properties of the dielectric surfaces allow for moving of the filaments, from time to time there are collisions between them resulting in the additional annihilation of one of the collision partners. If the driving voltage decreases below $\hat{U} \approx 269$ V discharge extinguishes.

From the above follows that the system exhibits hysteresis in the voltage interval between the extinction and ignition voltage. If this interval is entered from lower voltages no gas discharge will be ignited. Even if the system contains some ignited filaments an increase of the voltage within this interval will not re-ignite new filaments. To generate new filaments it is always necessary to exceed the ignition voltage. A similar hysteretic behaviour is known from in the pattern formation process in planar DC gas discharge systems. However, in DBD systems the hysteresis originates from the role of surface charges, as it will be seen later, whereas in DC systems the current-voltage characteristic of the discharge causes the hysteresis [15,19].

To obtain a single filament, first, the system is driven above the ignition voltage. And many filaments are ignited. This corresponds to a loose arrangement of filaments (pattern L, Fig. 3c). Then, the driving voltage is decreased to drive the system to the regime of single filaments S, Figure 3a. If one now waits for a few ten seconds filaments are annihilated spontaneously or via collisions. Finally, in general a single filament is left that may be stabilised by a small increase of the driving voltage of the order of some ten volts.

[1] For the rest of this article we want to consider a pattern to be static or stationary if the breakdown behaviour does not change in time and space from period to period.

3 The model

In this work we use a classical reaction-drift-diffusion model (often simply called drift-diffusion model) assuming charge transport due to electrons and one type of ions. Any further plasma chemistry is neglected. Therefore the evolution of the particle densities of electrons n_e and ions n_p is given in terms of two continuity equations. In the case of helium for which we want to present the numerical solutions we assume as ions He^+. The electric field E is calculated from volume and surface charges self-consistently via the Poisson equation

$$\partial_t n_{e,p} + \nabla \cdot \mathbf{\Gamma}_{e,p} = S_{e,p}, \tag{1}$$

$$\mathbf{\Gamma}_{e,p} = \mp\, n_{e,p}\, \mu_{e,p}(E)\mathbf{E} - D_{e,p}(E)\nabla n_{e,p}, \tag{2}$$

$$\varepsilon_0\, \varepsilon_r \nabla^2 \Phi = e(n_p - n_e), \qquad \mathbf{E} = -\nabla\Phi. \tag{3}$$

The mobilities of electrons μ_e and ions μ_p depend on the reduced electric field (local field approximation) and are tabulated [6,12]. The diffusion constants for electrons D_e and ions D_p are taken from Einstein's relation $D_{e,p} = \mu e, pkTe, p/e$ with an electron temperature of 2 eV and a gas (ion) temperature of 0.025 eV. The permittivity ε is 1 for the gas and 7.6 for the dielectric layers.

As we regard only one ion species, the source terms S_e and S_p are equal. They comprise solely the direct impact ionisation in the gas volume. The ionisation coefficient α depends on the reduced electric field, the values are also tabulated [12].

The current of ions that hit the dielectric surfaces generates secondary electrons and contributes to the surface charge. Each ion hitting the dielectric surface is supposed to be discharged and therefore delivers one elementary charge. The secondary emission coefficient γ is set to 0.05 as in previous calculations [16]. The electron current onto the dielectric surfaces contributes to the surface charges as every electron simply sticks to the surface. Surface charges of opposite sign introduced by ions and electrons annihilate each other. Boundaries of the discharge area that are not covered with dielectric surfaces are treated with Neumann zero flux boundary conditions.

The model equations are numerically solved with the 3-dimensional version of the software [2]. The same program has been successfully used in [16] to describe the evolution to a self-organised pattern in the form of a stable dense filament arrangement. A 2-dimensional variant of the model was used to describe plasma-display-panels [10, 13]. Here the model is applied to investigate a single stationary filament.

The simulation domain is shown in Figure 4. It consists of two dielectric layers and the gas gap. The electrodes cover the whole surface. The working gas has a pressure p of 200 hPa. The sinusoidal driving voltage with amplitude $\hat{U} = 400$ V is applied to the electrodes.

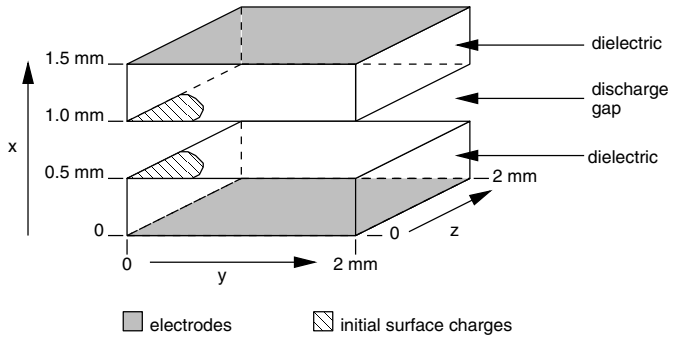

Fig. 4. The simulation domain consists of two dielectric layers and the gas gap. The electrodes cover the whole surface. Initially there are surface charges deposited on the inner surfaces to initiate the current filament. The system is mirrored in y and z-direction by zero flux boundary conditions. The numerical resolution is $x \times y \times z = 60 \times 60 \times 60$ in space and 0.5 ns in time.

The experimental transients leading to a single filament lasts a few seconds, i.e. some thousands of driving periods and therefore is out of reach for numerical simulations. Therefore we have chosen the approach to introduce an initial surface charge which is in shape and size near the expected self organised filament. The initial surface charge distribution σ has a Gaussian shape given by

$$\sigma = \sigma_{\max} \exp(-r^2/2r_0^2) \tag{4}$$

and the signs of the charges are opposite on the two dielectric surfaces. The values of $\sigma_{\max}$ and r_0 are estimated from the experiment. The centre of the initial charge distribution is positioned into one corner of the discharge area, as it is seen in Figure 4. Due to the mirroring through the boundary conditions this corresponds to a full, round charge distribution. As in the experiment, the driving voltage is chosen to be below the ignition voltage to avoid ignition that is spread over the discharge area.

3.1 Numerical results

In Figure 5 the results of numerical simulations for two initial charge distributions are shown. According to equation (4) they both have a hight of $\sigma_{\max} = 7$ nC/cm^2, but differ in their width, which is $r_0 = 0.5$ mm and $r_0 = 0.3$ mm respectively. The sinusoidal driving voltage has an amplitude of 400 V in both cases. In the beginning of the run, in both simulations the surface charge distribution undergoes noticeable changes after every breakdown. However, after approximately 12 breakdowns, the surface charge distribution does not change significantly any more, and the steady state being approximated is nearly identical in both simulations. To assure the stability of the steady state, both simulations are continued another 12 breakdowns. In Figure 5 the surface charge distributions after 24 breakdowns are shown. Notice, that the area occupied by the current filament is much smaller than the discharge area.

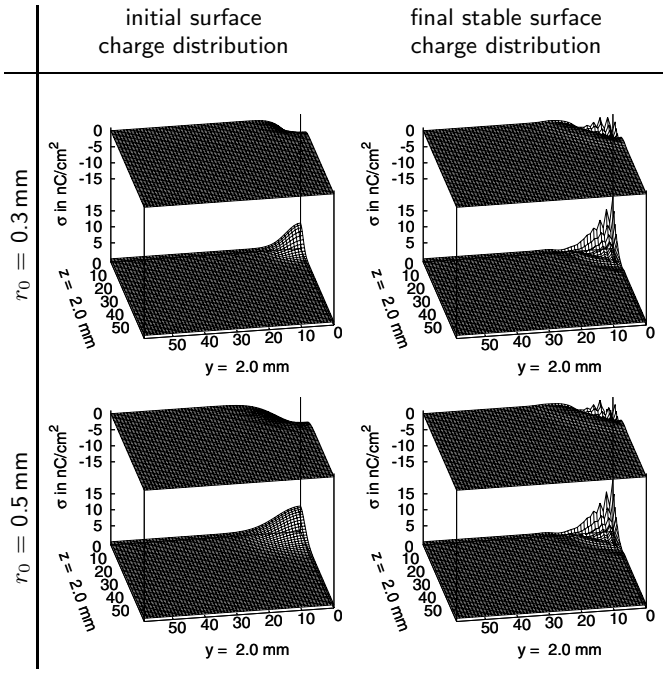

Fig. 5. Charge density distribution σ on the dielectric surfaces. The development of two different initial surface charge distributions (according to Eq. (4): $r_0 = 0.5$ mm, $\sigma_{\max} = 7$ nC/cm^2 and $r_0 = 0.3$ mm, $\sigma_{\max} = 7$ nC/cm^2) is shown. The stable surface charge distribution is the state reached after 24 breakdowns. The two filaments do not differ in size or shape any more.

If the initial surface charge density is chosen to be far away from that of the self-organised filament in the simulation we could not reach a final stationary stable filament state. If the initial surface charge distribution is much broader than the self-organised filament, the discharge splits up into several filaments. Note that this process can not be described in a radial (r, z) coordinate system. If the initial surface charge distribution is too small, the filament does not ignite.

The driving voltage and the results of the simulations for the real current are shown in Figure 6a. They are in rather good agreement with the experimental curves shown in Figure 2. A quantitative comparison of experimental and numerical data is given in Table 1. The physical parameters in both cases were the same, and both systems were driven below ignition voltage $\hat{U}_i$. The agreement of experimental and numerical data is very good. Hence, we conclude that our basic reaction-drift-diffusion model comprises all important physical effects necessary to describe self organised filaments in glow mode DBD.

3.2 Mechanism of stabilisation

We want to demonstrate in this chapter that the numerical simulations also allow for some insight into the mechanisms being responsible for the stabilisation of the current filaments in DBD systems of the kind that are used in the experimental part of this article. The role of surface

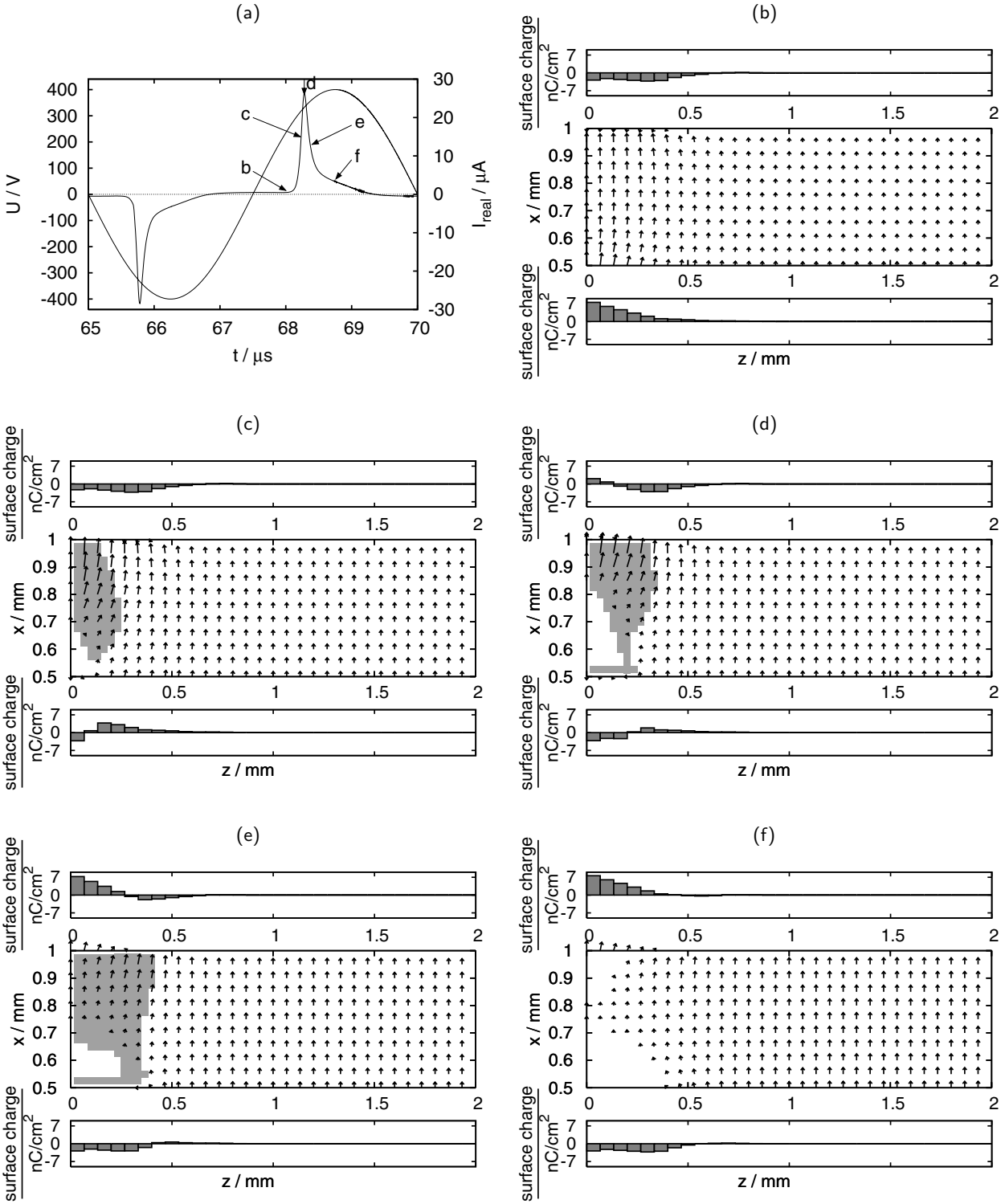

Fig. 6. Surface charge distribution and electrical field during a breakdown. The graphs (b)–(f) each comprise three parts; the upper and lower part show the smoothed surface charge distribution on the upper and lower electrode respectively. In between the discharge gap is shown, containing arrows depicting the electric field. In regions where the electric field is below 400 V/mm, no arrows are drawn. Grey shaded areas indicate a net positive volume charge of more than 10^{11} e/cm^3. The data are generated by a 3D calculation starting with a charge density distribution given by $r_0 = 0.5$ mm and $\sigma_{\max} = 7$ nC/cm^2 in equation (4). (b–f) Depict a cut along the x-z-plane at $y = 0$. Graph (a) shows the driving voltage and the real current in the simulation. The arrows indicate the times for graphs (b–f).

Table 1. Comparison of experimental and numerical results. Experimental parameters as in Figure 2, pattern type L according to Figure 3. Numerical parameters as in Figure 6. The experimental filament diameter is taken as double variance of the luminescence distribution, the corresponding numerical value is the double variance of the ion density distribution averaged over one half-cycle. The breakdown voltage refers to the onset of the breakdown in the steady state, e.g. the point a in Figure 6a.

	Experiment	Numeric
filament diameter (double variance)	0.61 mm	0.52 mm
real current pulse FWHM	100 ns	110 ns
charge per filament	20 pC	12 pC
breakdown voltage	200 V	320 V

charges in the filamentation process has been discussed qualitatively in [4]. In the present work, we support this argumentation with quantitative data and furthermore extend the mechanism by including the important influence of space charges.

To get insight into the processes being associated with the formation of current filaments, several states during a breakdown are depicted in Figure 6. Although the calculations were performed in three dimensions, for a simplicity a 2-dimensional cut in the x-z-plane at $y = 0$ is shown. To avoid numerical artefacts (that yield to the rough shape in the surface plots in Fig. 5) the surface charges are smoothed in Figure 6. The initial surface charge had a distribution that is described by $r_0 = 0.5$ mm and $\sigma_{\max} = 7$ nC/cm^2 in equation (4). The pictures are obtained after 28 breakdowns.

The arrows in Figure 6a depict the times for which the state of the discharge is drawn in Figures 6b–6f. Figure 6b shows the state of the system shortly before the onset of the breakdown. The surface charges are the result of the last breakdown and hence depict the former position of the filament. The lower dielectric is covered with positive surface charge, the upper dielectric with negative one. The electrode above the discharge gap is the temporary cathode, the electrode below is the temporary anode. The force on the electrons (i.e. the negative electric field $-\mathbf{E}$) is largest in the centre of the filament. This is because the electric field from the surface charges enhances the electric field from the external power supply. Consequently, breakdown starts at the centre of the filament of the preceding breakdown.

In the course of time, the driver voltage, and hence the voltage over the discharge gap, increases. Thus, the breakdown voltage is reached also in the surrounding of the filament centre. However, the filament does not grow arbitrarily in size. That is for two reasons. First, as long as there is no contribution to the voltage drop from the surface charges far away from the centre of the foregoing filament, a self-sustaining discharge does not take place. Second, there is a self-focusing effect of electrons into the filament centre induced by the volume charges occurring in the filament. In Figure 6 the sites in the discharge gap with a positive volume charge (i.e. $e(n_p - n_e)$) of more than 10^{11} e/cm^3 are shaded. In Figures 6c and 6d, depicting the beginning and the middle of the breakdown, the force on the electrons at the filament border points in direction to the filament. At the end of the breakdown in Figure 6e the focusing force becomes weaker but does not vanish. Especially in the second half of the breakdown (Figs. 6d and 6e) this opposes the effect expected from the surface charges, as they have changed their sign in the filament centre and hence reject electrons.

The self-focusing of electrons within the filament drains electrons from the filaments surrounding. Hence, a breakdown near a filament becomes inhibited. The self-focusing of electrons is also reflected in the particle density distributions, which is 0.52 mm (double variance) wide for ions but only 0.22 mm wide for electrons. Notice, that in a discharge driven above ignition voltage the self-focusing of electrons is the only effect preventing the direct surrounding from breakdown. Therefore, the self-focusing effect of the volume charges is essential to understand the filamentation in that case.

After breakdown has taken place, in Figure 6f, the surface charge distribution is the same as before the breakdown in Figure 6b with the two dielectric surfaces exchanged with respect to each other. The external electric field from the driver now is weakened by the surface charges, and the gap voltage is too small to sustain the discharge.

4 Conclusion

In the experimental part (Sect. 2) of this article we introduced a planar dielectric barrier discharge system which is known to exhibit self-organised patterns in the current distribution of the discharge plane. In general the discharge is filamentary and leads to a single real current peak per half-cycle of the driving voltage. We gave a systematic overview of the most commonly observed filamentary patterns, thereby particular emphasis has been put on the parameter range where hysteresis is observed. We pointed out a way to prepare a single filament experimentally. In a wide range of parameters the filaments have a diameter of order of 1 mm and do not change their shape.

In the theoretical part (Sect. 3) we used a classical reaction-drift-diffusion model that is known to be able to describe the filamentation processes [16]. In this article we proved that the same model also describes single isolated filaments in the sense of a stationary state over many breakdowns. The model predictions of filament diameter, duration of the breakdown, and charge transfer per filament agree quite well with the experimental findings. Last not least, we explained the mechanism of filament stabilisation in glow mode due to the interplay of surface charges and focusing volume charges which is significantly different from commonly known filamentation mechanisms in spark discharges.

This work was financially supported by DAAD and DFG.

References

1. E. Ammelt, D. Schweng, H.-G. Purwins, Phys. Lett. A **179**, 348 (1993)
2. J.-P. Boeuf, L.C. Pitchford, W.L. Morgan, SIPDP, Kinema Research, Monument, CO, 1997, `http://www.siglo-kinema.com/`
3. I. Brauer, C. Punset, H.-G. Purwins, J.P. Boeuf, J. Appl. Phys. **85**, 7569 (1999)
4. W. Breazeal, K.M. Flynn, E.G. Gwinn, Phys. Rev. E **52**, 1503 (1995)
5. L. Dong, Z. Yin, L. Wang, G. Fu, Y. He, Z. Chai, X. Li, Thin Solid Films **435**, 120 (2003)
6. H.W. Ellis, R.Y. Pai, E.W. McDaniel, E.A. Mason, L.A. Viehland, At. Data Nucl. Data Tables **17**, 177 (1976)
7. E.L. Gurevich, A.L. Zanin, A.S. Moskalenko, H.-G. Purwins, Phys. Rev. Lett. **91**, 154501 (2003)
8. U. Kogelschatz, B. Eliasson, W. Egli, Pure Appl. Chem. **71**, 1819 (1999)
9. S. Matern, V.M. Marchenko, Y.A. Astrov, L.M. Portsel, H.-G. Purwins, Proc. SPIE **4669**, 13 (2002)
10. J. Meunier, P. Belenguer, J.P. Boeuf, J. Appl. Phys. **78**, 731 (1995)
11. I. Müller, C. Punset, E. Ammelt, H.-G. Purwins, J.P. Boeuf, IEEE Trans. Plasma Sci. **27**, 20 (1999)
12. L.C. Pitchford, J.-P. Boeuf, W.L. Morgan, BOLSIG, a user-friendly boltzmann solver, Kinema Research, Monument, CO, 1996, `http://www.siglo-kinema.com/`
13. C. Punset, J.P. Boeuf, L.C. Pitchford, J. Appl. Phys. **83**, 1884 (1998)
14. I. Radu, R. Bartnikas, M.R. Wertheimer, J. Appl. Phys. **95**, 5994 (2004)
15. Y.P. Raizer, U. Ebert, D.D. Šijačić, Phys. Rev. E **70**, 017401 (2004)
16. L. Stollenwerk, Sh. Amiranashvili, J.-P. Boeuf, H.-G. Purwins, Phys. Rev. Lett. **96**, 255001 (2006)
17. L. Stollenwerk, Sh. Amiranashvili, H.-G. Purwins, New J. Phys. **8**, 217 (2006)
18. L. Stollenwerk, H.-G. Purwins, Europhys. Lett. **70**, 22 (2005)
19. D.D. Šijačić, U. Ebert, Phys. Rev. E **66**, 1 (2002)